Frascati Physics Series Vol. 69 (2019)
PHOTON 2019 - International Conference on the Structure and the Interactions of the Photon
Jun 3-7, 2019

TWO-PHOTON FUSION HIGGS PRODUCTION IN COLLISIONS WITH PROTON AND ION BEAMS AT THE LHC, HE-LHC, AND FCC

David d'Enterria
CERN, EP Department, 1211 Geneva, Switzerland
Daniel E. Martins
UFRJ, Univ. Federal do Rio de Janeiro, 21941-901, Rio de Janeiro, RJ
Patricia Rebello Teles
ERJ, Univ. do Estado do Rio de Janeiro, 20550-900, Rio de Janeiro, RJ

Abstract

The production of the Higgs boson in ultraperipheral collisions (UPCs) of proton and nuclear beams at three future colliders — the high-luminosity Large Hadron Collider (HL-LHC), the high-energy LHC (HE-LHC), and the Future Circular Collider (FCC) — is studied. The cross sections for the process $AA \xrightarrow{\gamma\gamma} (A)H(A)$, with the Higgs particle produced via two-photon fusion at midrapidity and the hadron(s) A surviving the interaction, are computed with MADGRAPH 5 extended with the corresponding coherent γ fluxes for Pb-Pb, Xe-Xe, Kr-Kr, Ar-Ar, O-O, p-Pb, and p-p collisions over $\sqrt{s_{_{NN}}} \approx 3$–100 TeV. Taking into account the expected luminosities for all colliding systems, the yields and significances for observing the Higgs boson in UPCs, on top of the $\gamma\gamma \to b\bar{b}, c\bar{c}, q\bar{q}$ continuum backgrounds, at the three future colliders are estimated. At HL-LHC and HE-LHC, the systems with larger Higgs significance are Ar-Ar(6.3 TeV) and Kr-Kr(12.5 TeV) respectively. However, evidence for $\gamma\gamma \to H$ production would require $\times 200$ and $\times 30$ times larger integrated luminosities at both machines. Factors of ten can be gained by running for a year, rather than the typical 1-month heavy-ion run at the LHC, but the process will likely remain unobserved unless a higher energy collider such as the FCC is built. In the latter machine, a 5σ observation of $\gamma\gamma \to H$ is warranted in just the first nominal Pb-Pb and p-Pb runs.

1 Introduction

Heavy ions accelerated at high energies are surrounded by huge electromagnetic (e.m.) fields generated by the collective action of their Z individual proton charges. In the equivalent photon approximation (EPA) [1], such strong e.m. fields can be identified as quasireal photon beams with very low virtualities $Q^2 < 1/R_A^2$ and large longitudinal energies of up to $\omega_{\max} \approx \gamma_L/R_A$, where R_A is the radius of the emitting charge and $\gamma_L = E_{\rm beam}/m_{N,p}$ is the beam Lorentz factor for nucleon or proton mass $m_{N,p} =$ 0.9315, 0.9382 GeV [2, 3]. On the one hand, since the photon flux scales as the squared charge of

each colliding particle, photon-photon cross sections are enhanced millions of times for heavy ions (up to $Z^4 \approx 5 \cdot 10^7$ for Pb-Pb) compared to proton or electron beams. On the other hand, proton (and lighter ions) feature larger $\omega_{\rm max}$ values thanks to their lower radii R_A and larger beam γ_L factors, and can thereby reach higher photon-photon c.m. energies. At LHC energies, photons emitted from nuclei (with radii $R_A \approx 1.2\,A^{1/3}$ fm) are almost on-shell (virtuality $Q < 0.06$ GeV, for mass numbers $A > 16$), and reach longitudinal energies of up to hundreds of GeV, whereas photon fluxes from protons ($R_A \approx 0.7$ fm) have larger virtualities, $Q \approx 0.28$ GeV, and longitudinal energies in the TeV range [3]. Table 1 summarizes the relevant characteristics of $\gamma\,\gamma$ collisions in ultraperipheral collisions (UPCs) of proton and nuclear beams at the HL-LHC, HE-LHC, and FCC. The beam-beam luminosities are from the estimates of Refs. [4, 5], whereas for p-p collisions, we take $\mathscr{L}_{\rm int} = 1$ fb^{-1} as the value potentially integrated under low-pileup conditions that allow for exclusive $\gamma\,\gamma$ measurements. One can see that, in all cases, the maximum photon-photon c.m. energies reach above the kinematical threshold for Higgs boson production, $\sqrt{s^{\rm max}_{\gamma\,\gamma}} \gtrsim m_{\rm H} = 125\,{\rm GeV}$.

Table 1: Main features of photon-photon collisions in UPCs with proton and nuclear beams at the HL-LHC, HE-LHC, and FCC: (i) Nucleon-nucleon c.m. energy $\sqrt{s_{\rm NN}}$, (ii) integrated luminosity per run $\mathscr{L}_{\rm int}$, (iii) beam energies $\rm E_{beam}$, (iv) Lorentz factor γ_L, (v) effective charge radius R_A, (vi) photon "maximum" energy $\omega_{\rm max}$ in the c.m. frame, and (vii) "maximum" photon-photon c.m. energy $\sqrt{s^{\rm max}_{\gamma\,\gamma}}$. The last two columns list the $\gamma\,\gamma \to$ H cross sections and number of events expected for the quoted $\mathscr{L}_{\rm int}$ per system.

System	$\sqrt{s_{\rm NN}}$	$\mathscr{L}_{\rm int}$	$E_{\rm beam1} + E_{\rm beam2}$	γ_L	R_A	$\omega_{\rm max}$	$\sqrt{s^{\rm max}_{\gamma\,\gamma}}$	$\sigma(\gamma\gamma \to {\rm H})$	$\rm N(\gamma\gamma \to H)$
Pb-Pb	5.5 TeV	10 nb^{-1}	2.75 + 2.75 TeV	2950	7.1 fm	80 GeV	160 GeV	15 pb	0.15
Xe-Xe	5.86 TeV	30 nb^{-1}	2.93 + 2.93 TeV	3150	6.1 fm	100 GeV	200 GeV	7 pb	0.21
Kr-Kr	6.46 TeV	120 nb^{-1}	3.23 + 3.23 TeV	3470	5.1 fm	136 GeV	272 GeV	3 pb	0.36
Ar-Ar	6.3 TeV	1.1 pb^{-1}	3.15 + 3.15 TeV	3400	4.1 fm	165 GeV	330 GeV	0.36 pb	0.40
O-O	7.0 TeV	3.0 pb^{-1}	3.5 + 3.5 TeV	3750	3.1 fm	240 GeV	490 GeV	35 fb	0.11
p-Pb	8.8 TeV	1 pb^{-1}	7.0 + 2.75 TeV	7450, 2950	0.7, 7.1 fm	2.45 TeV, 130 GeV	2.6 TeV	0.17 pb	0.17
p-p	14 TeV	1 fb^{-1}	7.0 + 7.0 TeV	7450	0.7 fm	2.45 TeV	4.5 TeV	0.18 fb	0.18
Pb-Pb	10.6 TeV	10 nb^{-1}	5.3 + 5.3 TeV	5700	7.1 fm	160 GeV	320 GeV	150 pb	1.5
Xe-Xe	11.5 TeV	30 nb^{-1}	5.75 + 5.75 TeV	6200	6.1 fm	200 GeV	400 GeV	60 pb	1.8
Kr-Kr	12.5 TeV	120 nb^{-1}	6.25 + 6.25 TeV	6700	5.1 fm	260 GeV	530 GeV	20 pb	2.4
Ar-Ar	12.1 TeV	1.1 pb^{-1}	6.05 + 6.05 TeV	6500	4.1 fm	320 GeV	640 GeV	1.7 pb	1.9
O-O	13.5 TeV	3.0 pb^{-1}	6.75 + 6.75 TeV	7300	3.1 fm	470 GeV	940 GeV	0.11 pb	0.33
p-Pb	18.8 TeV	1 pb^{-1}	13.5 + 5.3 TeV	14 400, 5700	0.7, 7.1 fm	4.1 TeV, 160 GeV	4.2 TeV	0.45 pb	0.45
p-p	27 TeV	1 fb^{-1}	13.5 + 13.5 TeV	14 400	0.7 fm	4.1 TeV	8.2 TeV	0.30 fb	0.30
Pb-Pb	39 TeV	110 nb^{-1}	19.5 + 19.5 TeV	21 000	7.1 fm	600 GeV	1.2 TeV	1.8 nb	200
p-Pb	63 TeV	29 pb^{-1}	50. + 19.5 TeV	53 300, 21 000	0.7,7.1 fm	15.2 TeV, 600 GeV	15.8 TeV	1.5 pb	45
p-p	100 TeV	1 fb^{-1}	50. + 50. TeV	53 300	0.7 fm	15.2 TeV	30.5 TeV	0.70 fb	0.70

The possibility to produce the Higgs boson by exploiting the huge photon field in UPCs of ions, $\rm AA \xrightarrow{\gamma\gamma} (A)H(A)$, where the scalar boson is produced at midrapidities and the colliding ions (A) survive their electromagnetic interaction (first diagram in Fig. 1 top-right), was first considered in several studies 30 years ago [6]. The observation of such $\gamma\,\gamma \to$ H process would provide an independent measurement of the H–γ loop-induced coupling based not on Higgs decays but on its s-channel production mode, as well as a model-independent extraction of the total Higgs width combining this process with the $\rm H \to \gamma\,\gamma$ decay channel measured at future $\rm e^+e^-$ Higgs factories. Detailed studies of the actual measurement of the Higgs boson in its dominant $\rm b\bar{b}$ decay mode, including realistic experimental acceptance and efficiencies for the signal and the $\gamma\,\gamma \to \rm b\bar{b}, c\bar{c}, q\bar{q}$ continuum backgrounds (second diagram in Fig. 1 top-right), were first presented in Ref. [7] for ultraperipheral proton-nucleus (p-A) and nucleus-nucleus (A-A) collisions at LHC energies. This work showed that, for the nominal integrated luminosities, the scalar boson was unobservable in UPCs at the LHC unless one integrated at least $\times$300 times more luminosity than that expected for the standard 1-month heavy-ion operation. Although the LHC beam luminosities for p-p are 7 orders of magnitude larger than for Pb-Pb, the running conditions with 50 or more pileup p-p

collisions per bunch crossing make it impossible to select exclusive photon-photon events with central masses at 125-GeV unless one installs very forward proton taggers (at 420 m inside the LHC tunnel) with 10-picosecond time resolution [8]. On the other hand, similar studies [9] carried out within the CERN Future Circular Collider (FCC) project [5], indicated that the observation of Higgs production in UPCs was clearly possible in just the first nominal run of Pb-Pb and p-Pb collisions at $\sqrt{s_{_{\rm NN}}} = 39$ and 63 TeV respectively. This writeup provides a summary of the more detailed studies reported in Ref. [10] for a Higgs boson measurement in the High-Luminosity phase of the LHC (HL-LHC), as well as at the proposed High-Energy LHC (HE-LHC) with twice larger c.m. energies [4], including not only higher luminosities but also collisions of lighter ions (Xe-Xe, Kr-Kr, Ar-Ar, O-O).

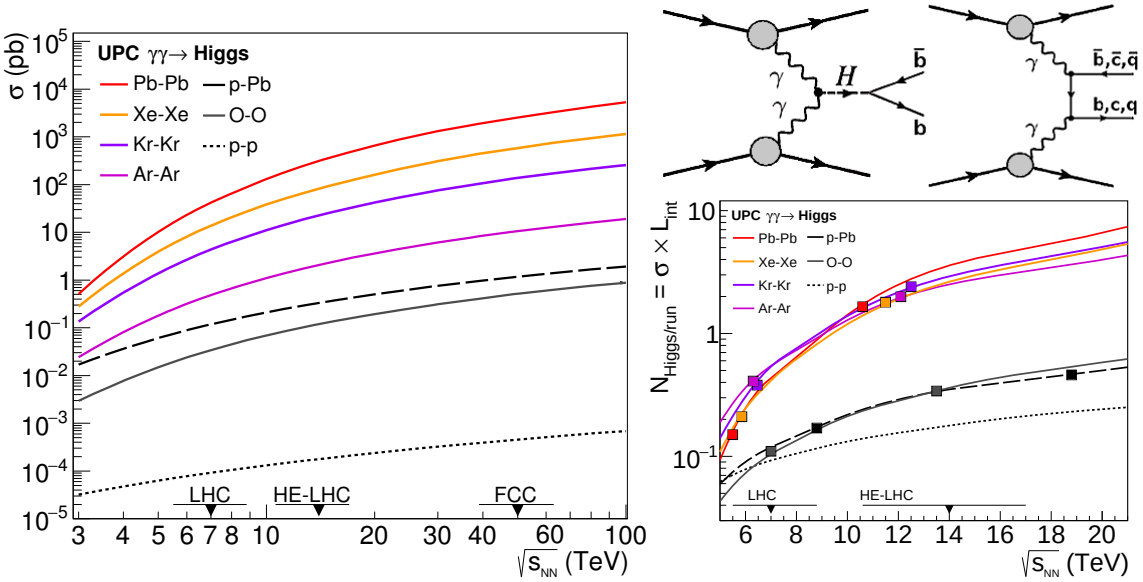

Figure 1: *Left: Two-photon fusion Higgs boson cross section versus nucleon-nucleon c.m. energy in nuclear and proton collisions over* $\sqrt{s_{_{\rm NN}}}$ *= 3–100 TeV. Right-top: Diagrams for the two-photon production of the Higgs boson (*$\rm b\bar{b}$ *decay) and of the b-,c-,light-quark pair backgrounds. Right-bottom: Number of Higgs bosons produced per month in UPCs of various colliding systems in the HL-LHC/HE-LHC energy range.*

2 Theoretical setup

The MADGRAPH 5 (v.2.5.4) Monte Carlo (MC) event generator [11] is employed to compute the UPC Higgs boson cross sections, following the implementation discussed in detail in [7], from the convolution of the Weizsäcker-Williams EPA photon fluxes for the proton and/or ions, and the elementary $\gamma\,\gamma \to {\rm H}$ cross section (with H-γ coupling parametrized in the Higgs effective field theory [12]):

$$\sigma_{{\rm A_1A_2}\to{\rm H}} = \int dm_{\rm H}\, dy_{\rm H}\, \frac{2m_{\rm H}}{s}\, f_{\gamma/A_1}(x_1) f_{\gamma/A_2}(x_2)\, \hat{\sigma}_{\gamma\,\gamma\to{\rm H}}\ ; \tag{1}$$

where $x = \omega/E$ is the beam energy fraction carried by the photon. For protons, the MADGRAPH 5 default γ flux is given by the energy spectrum of Ref. [13]:

$$f_{\gamma/p}(x) = \frac{\alpha}{\pi}\, \frac{1 - x + 1/2x^2}{x} \int_{Q^2_{\rm min}}^{\infty} \frac{Q^2 - Q^2_{\rm min}}{Q^4} |F(Q^2)|^2 dQ^2\ , \tag{2}$$

where $\alpha = 1/137$, $F(Q^2)$ is the proton e.m. form factor, and the minimum momentum transfer $Q_{\rm min}$ is a function of x and the proton mass m_p, $Q^2_{\rm min} \approx (x\,m_p)^2/(1-x)$. For ions of charge Z, the photon energy spectrum, integrated over impact parameter b from $b_{\rm min} = R_A$ to infinity, is [14]:

$$f_{\gamma/A}(x) = \frac{\alpha\,Z^2}{\pi}\,\frac{1}{x}\left[2x_i K_0(x_i)K_1(x_i) - x_i^2(K_1^2(x_i) - K_0^2(x_i))\right], \qquad (3)$$

where $x_i = x\,m_N\,b_{\rm min}$, K_0, K_1 are the zero- and first-order modified Bessel functions of the second kind, and for the different nuclear radii R_A, we use the data from elastic lepton-nucleus collisions [15]. We exclude nuclear overlap by imposing $b_1 > R_{A_1}$ and $b_2 > R_{A_2}$ for each photon flux, and applying a correcting factor on the final cross section that depends on the ratio of Higgs mass over $\sqrt{s_{\rm NN}}$ [16].

After cross section determination, the event generation is carried out for the dominant Higgs decay mode, $\rm H \to b\bar{b}$ with 56% branching fraction [17], as it is the final state that provides the largest number of signal events. The same setup is used to generate the exclusive two-photon production of $\rm b\bar{b}$ and (misidentified) $\rm c\bar{c}$ and light-quark ($\rm q\bar{q}$) jet pairs, which constitute the most important physical backgrounds for the $\rm H \to b\bar{b}$ measurement. For the HL-LHC and HE-LHC system, the analysis is carried out at the parton level only, whereas for FCC energies, we have further used PYTHIA 8.2 [18] to shower and hadronize the two final-state b-jets generated, which are then reconstructed with the Durham k_t algorithm [19] (exclusive 2-jets final-state) using FASTJET 3.0 [20].

3 Total Higgs cross sections

The ultraperipheral Higgs boson cross sections as a function of $\sqrt{s_{\rm NN}}$ are shown in Fig. 1 (left) and listed in the before-last column of Table 1 for all p-p, p-A, and A-A systems considered. The theoretical cross sections have a conservative 20% uncertainty (not quoted) to cover different charge form factors and nuclear overlap conditions. As expected, the bigger the charge of the colliding ions the larger the UPC cross sections, but such advantage is mitigated by the correspondingly reduced beam-beam luminosities for heavier ions. Figure 1 (right-bottom) shows the product of Higgs UPC cross section times the integrated luminosities for each colliding system in the HL-LHC and HE-LHC energy range. At the LHC, we see that, despite the fact that Pb-Pb features the largest Higgs cross section, $\sigma(\gamma\,\gamma \to {\rm H}) = 15$ pb, there are about 2.5 times more scalar bosons per month in Ar-Ar and Kr-Kr collisions (0.40 versus 0.15, last column of Table 1) thanks to the comparatively larger luminosities and c.m. energies of the latter compared to lead beams. At HE-LHC, the Higgs cross sections are about a factor of 10 larger than at the LHC, and most colliding systems feature 1.5–2.5 Higgs bosons produced per month. The most competitive systems to try a measurement of UPC Higgs production are Ar-Ar and Kr-Kr at HL-LHC and HE-LHC respectively. At the FCC, the cross sections are two orders of magnitude larger than at the LHC, reaching $\sigma(\gamma\,\gamma \to {\rm H}) = 1.75$ nb and 1.5 pb in Pb-Pb and p-Pb collisions at $\sqrt{s_{\rm NN}} = 39$ and 63 TeV which, for the nominal $\mathscr{L}_{\rm int} = 110$ nb^{-1} and 29 pb^{-1} per-month integrated luminosities, yield ∼200 and 45 Higgs bosons produced (corresponding to 110 and 25 bosons in the $\rm b\bar{b}$ decay mode, respectively).

4 Data analysis and Higgs boson significances

The observation of the Higgs boson in UPCs relies on the measurement of two exclusive b-jets with invariant masses peaked at $m_{\rm H}$, on top of a background of $\gamma\gamma \to \rm b\bar{b}, c\bar{c}, q\bar{q}$ continuum pairs, where charm and light (q = u, d, s) quarks are misidentified as b-quarks. For all colliding systems and at all $\sqrt{s_{\rm NN}}$, the pure MC-level background continuum cross sections over $m_{\rm H} \approx 100$–150 GeV, computed with the same MADGRAPH 5 setup, are about 25, 200, and 10^3 times larger respectively than the Higgs signal.

The data analysis follows closely the study of Ref. [7], with the following acceptance and reconstruction performances assumed: jet reconstruction over $|\eta| < 2.5$ (< 5 for FCC), 7% b-jet energy resolution (resulting in a dijet mass resolution of ∼6 GeV at the Higgs peak), 70% b-jet tagging efficiency, and 5% (1.5%) b-jet mistagging probability for a c (light-flavour q) quark. For the double b-jet final-state of interest, these lead to a ∼50% efficiency for the MC-generated signal ($\mathscr{S}$), and a total reduction of the misidentified $c\bar{c}$ and $q\bar{q}$ continuum backgrounds ($\mathscr{B}$) by factors of ∼400 and ∼4500 respectively. The sum of remaining continuum backgrounds can be reduced through proper kinematical cuts: (i) requiring jets with $p_T \approx m_H/2 = 55$–67 GeV (as expected for jets from the decay of an UPC Higgs produced almost at rest) suppresses more than 95% of the continuum, while removing only half of the signal; (ii) requiring $|\cos\theta_{j_1 j_2}| < 0.5$ — to exploit the fact that the angular distribution in the helicity frame of the Higgs decay b-jets is isotropic while the continuum (with quarks propagating in the t- or u- channels) is peaked in the forward–backward directions — further suppresses the backgrounds while leaving almost untouched the signal; and (iii) the pair jet mass to be within $\pm 1.4\sigma_{jj}$ around the Higgs mass (i.e. $116 \lesssim m_{b\bar{b}} \lesssim 134$ GeV). For all systems, the overall loss of Higgs signal events due to the acceptance and kinematical cuts (i.e. without accounting for (mis)identification efficiencies) is around a factor of two, whereas the backgrounds are reduced by factors of 30 to 100, resulting in a final $\mathscr{S}/\mathscr{B} \approx 1$ for all colliding species.

Table 2: Summary of the cross sections after each event selection step, and final number of events expected (for the nominal integrated luminosities quoted) for signal and backgrounds in the $\gamma\gamma \to H(b\bar{b})$ measurements in Ar-Ar at HL-LHC, Kr-Kr at HE-LHC, and Pb-Pb and p-Pb at FCC.

Ar-Ar at $\sqrt{s_{_{NN}}} = 6.3$ TeV	cross section (b-jet (mis)tag effic.)	visible cross section after $\eta^j, p_T^j, \cos\theta_{jj}, m_{jj}$ cuts	N_{evts} ($\mathscr{L}_{int} = 1.1$ pb^{-1})
$\gamma\gamma \to H \to b\bar{b}$	0.20 pb (0.10 pb)	0.045 pb	0.05
$\gamma\gamma \to b\bar{b}$ [$m_{b\bar{b}}$=100–150 GeV]	8.2 pb (4.0 pb)	0.06 pb	0.06
$\gamma\gamma \to c\bar{c}$ [$m_{c\bar{c}}$=100–150 GeV]	60 pb (0.15 pb)	0.006 pb	0.006
$\gamma\gamma \to q\bar{q}$ [$m_{q\bar{q}}$=100–150 GeV]	70 pb (0.016 pb)	–	–
Kr-Kr at $\sqrt{s_{_{NN}}} = 12.5$ TeV			N_{evts} ($\mathscr{L}_{int} = 0.12$ pb^{-1})
$\gamma\gamma \to H \to b\bar{b}$	11 pb (5.5 pb)	2.5 pb	0.30
$\gamma\gamma \to b\bar{b}$ [$m_{b\bar{b}}$=100–150 GeV]	365 pb (180 pb)	2.8 pb	0.34
$\gamma\gamma \to c\bar{c}$ [$m_{c\bar{c}}$=100–150 GeV]	2.7 nb (6.7 pb)	0.24 pb	0.03
$\gamma\gamma \to q\bar{q}$ [$m_{q\bar{q}}$=100–150 GeV]	3.1 nb (0.70 pb)	–	–
Pb-Pb at $\sqrt{s_{_{NN}}} = 39$ TeV			N_{evts} ($\mathscr{L}_{int} = 110$ nb^{-1})
$\gamma\gamma \to H \to b\bar{b}$	1.0 nb (0.50 nb)	0.19 nb	21.1
$\gamma\gamma \to b\bar{b}$ [$m_{b\bar{b}}$=100–150 GeV]	24.3 nb (11.9 nb)	0.23 nb	25.7
$\gamma\gamma \to c\bar{c}$ [$m_{c\bar{c}}$=100–150 GeV]	525 nb (1.30 nb)	0.02 nb	2.3
$\gamma\gamma \to q\bar{q}$ [$m_{q\bar{q}}$=100–150 GeV]	590 nb (0.13 nb)	0.002 nb	0.25
p-Pb at $\sqrt{s_{_{NN}}} = 63$ TeV			N_{evts} ($\mathscr{L}_{int} = 29$ pb^{-1})
$\gamma\gamma \to H \to b\bar{b}$	0.87 pb (0.42 pb)	0.16 pb	4.8
$\gamma\gamma \to b\bar{b}$ [$m_{b\bar{b}}$=100–150 GeV]	21.8 pb (10.7 pb)	0.22 pb	6.3
$\gamma\gamma \to c\bar{c}$ [$m_{c\bar{c}}$=100–150 GeV]	410 pb (1.03 pb)	0.011 pb	0.3
$\gamma\gamma \to q\bar{q}$ [$m_{q\bar{q}}$=100–150 GeV]	510 pb (0.114 pb)	0.001 pb	0.04

Table 2 lists the cross sections after each event selection step, and final number of events expected (for the nominal integrated luminosities quoted) for signal and backgrounds in the systems with larger signal strength at each collider (Fig. 1, right-bottom): Ar-Ar at $\sqrt{s_{_{NN}}} = 6.3$ TeV, Kr-Kr at $\sqrt{s_{_{NN}}} = 12.5$ TeV, and Pb-Pb at $\sqrt{s_{_{NN}}} = 39$ TeV. Since the FCC case has been studied with more detail [9], we include also

in the table the results obtained in p-Pb at $\sqrt{s_{_{NN}}} = 63$ TeV. The Ar-Ar and Kr-Kr numbers quoted after each set of cuts are realistic estimates based on the overall signal and background losses derived in the complete MC studies of Refs. [7, 9]. The listed Pb-Pb and p-Pb results at FCC are those obtained in the full MC analysis described in Ref. [9]. The last column of Table 2 lists the final number of signal and background events expected after all selection criteria for the nominal 1-month run operation. The expected number of Higgs events per month, after cuts, at HL-LHC and HE-LHC are below unity and one would need to integrate at least factors of $\times$300 and $\times$20 more luminosities, respectively, in order to see a 3σ evidence of UPC Higgs production (Fig. 2). These factors are derived simply by requiring that the $\mathscr{S}/\sqrt{\mathscr{B}}$ ratio around the Gaussian Higgs peak ($116 < m_{\mathrm{b\bar{b}}} < 133$ GeV), is above 3. A factor of $\times$10 in $\mathscr{L}_{\mathrm{int}}$ could be gained by running for the time typical of a proton-proton run, instead of the nominal 1-month heavy-ion run operation. Such a longer run, motivated by Higgs- rather than heavy-ion physics, at HE-LHC would allow for an evidence of the process, by combining two experiments. Achieving the same significance at the HL-LHC seems out of reach, unless an extra factor of ten enhancement in the instantaneous Ar-Ar luminosity is accomplished by some (currently unidentified) means.

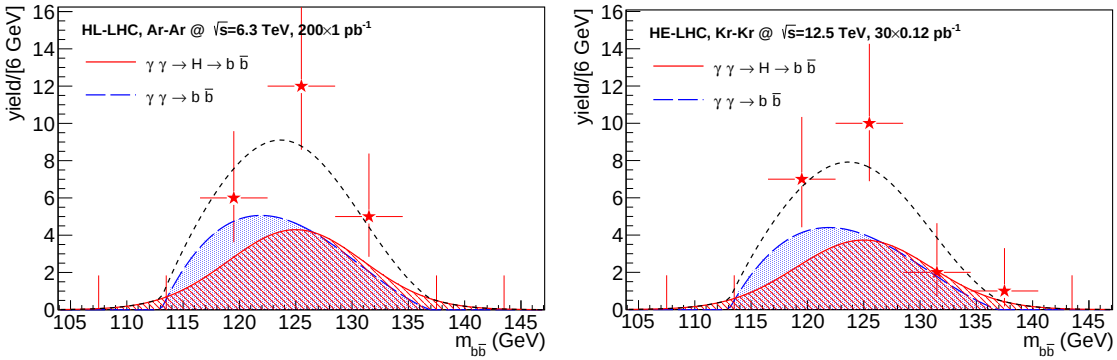

Figure 2: *Expected invariant mass distributions for b-jet pairs from two-photon-fusion Higgs signal (red Gaussian) over the* $\mathrm{b\bar{b}}+\mathrm{c\bar{c}}+\mathrm{q\bar{q}}$ *continuum (hatched blue area) in ultraperipheral Ar-Ar* ($\sqrt{s_{_{NN}}} = 6.3$ *TeV, left) and Kr-Kr* ($\sqrt{s_{_{NN}}} = 12.5$ *TeV, right) collisions, after event selection criteria with integrated luminosities* $\times 200$ *and* $\times 30$ *larger than the nominal ones for each system.*

At the FCC, Pb-Pb collisions at $\sqrt{s} = 39$ GeV with the integrated luminosity of $\mathscr{L}_{\mathrm{int}} = 110$ nb^{-1} per nominal 1-month run, results in about $\sim$21 signal counts over $\sim$28 for the sum of backgrounds in a window $m_{\mathrm{b\bar{b}}} = 116$–$133$ GeV around the Higgs peak. Reaching a statistical significance of 5σ (Fig. 3, right) would require to combine two different experiments (or doubling the luminosity in a single one). Similar estimates for p-Pb at 63 TeV (29 pb^{-1}) yield about 5 signal events after cuts, over a background of 6.7 continuum events. Reaching a 5σ significance for the observation of $\gamma\gamma \to \mathrm{H}$ production (Fig. 3, left) would require in this case to run for about 8 months (instead of the nominal 1-month run per year), or running 4 months and combining two experiments.

5 Conclusion

Prospective studies for the measurement of the two-photon production of the Higgs boson in the $\mathrm{b\bar{b}}$ decay channel in ultraperipheral Pb-Pb, Xe-Xe, Kr-Kr, Ar-Ar, O-O, p-Pb, and p-p collisions at the HL-LHC, HE-LHC, and FCC, have been presented. Cross sections have been obtained with MADGRAPH 5 including nuclear and proton equivalent photon fluxes and requiring no hadronic overlap of the colliding beams, at nucleon-nucleon c.m. energies over $\sqrt{s_{_{NN}}} = 5$–100 TeV. The same setup is used to generate

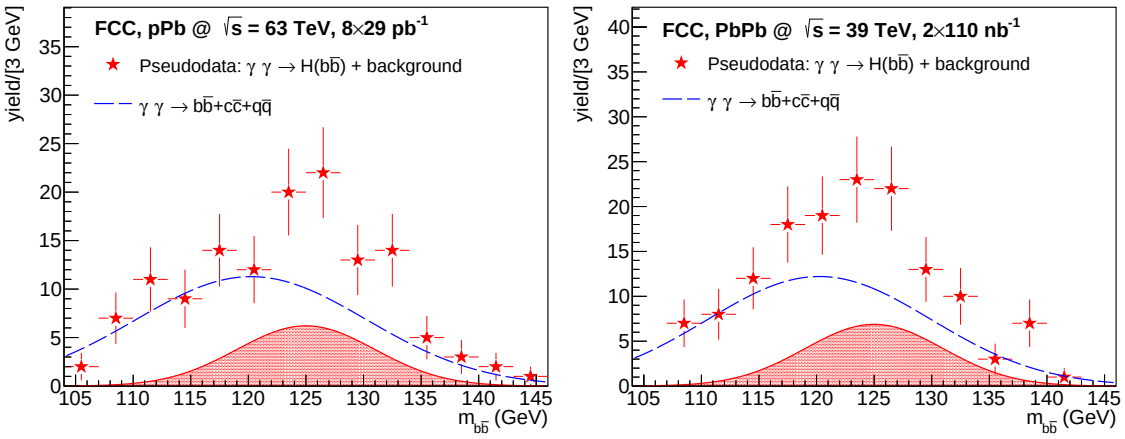

Figure 3: *Expected invariant mass distributions for b-jet pairs from two-photon-fusion Higgs signal (red Gaussian) over the* $\mathrm{b\bar{b}} + \mathrm{c\bar{c}} + \mathrm{q\bar{q}}$ *continuum (hatched blue area) in ultraperipheral p-Pb* ($\sqrt{s_{_{\mathrm{NN}}}} = 63$ *TeV, left) and Pb-Pb* ($\sqrt{s_{_{\mathrm{NN}}}} = 39$ *TeV, right) collisions, after event selection criteria with the quoted integrated luminosities (see text).*

the exclusive two-photon production of $\mathrm{b\bar{b}}$ and (misidentified) $\mathrm{c\bar{c}}$ and light-quark ($\mathrm{q\bar{q}}$) jet pairs, which constitute the most important physical backgrounds. By assuming realistic jet acceptance, reconstruction performances, and (mis)tagging efficiencies, and applying appropriate kinematical cuts on the jet p_T and angles in the helicity frame, we can reconstruct the $\mathrm{H(b\bar{b})}$ signal on top of the dominant $\gamma\,\gamma \to \mathrm{b\bar{b}}$ continuum background with $\mathscr{S}/\mathscr{B} \approx 1$ signal-over-background ratios. On the one hand, reaching 3σ evidence of UPC Higgs-production at HL-LHC and at HE-LHC, requires factors of about $\times 200$ and $\times 30$ more integrated luminosities in Ar-Ar and Kr-Kr collisions, respectively, than currently planned for both machines. Factors of ten in integrated luminosity can be gained running for the duration (10^7 s) typical of a p-p run, rather than the nominal 1-month heavy-ion operation, but would still fall too short for any feasible measurement at the HL-LHC. On the other hand, the measurement of $\gamma\,\gamma \to \mathrm{H} \to \mathrm{b\bar{b}}$ would yield about 20 (5) signal counts after cuts in Pb-Pb (p-Pb) collisions at the FCC for their nominal integrated luminosities per run. Observation of the two-photon-fusion Higgs production at the 5σ-level is thereby achievable in the first FCC run by combining the measurements of two experiments. The feasibility studies presented here indicate the Higgs physics potential opened up to study in $\gamma\gamma$ ultraperipheral ion collisions at current and future CERN hadron colliders, eventually providing an independent measurement of (i) the H-γ coupling not based on Higgs decays but on a s-channel production mode, as well as (ii) its total width by combining this $\gamma\,\gamma \to \mathrm{H}$ measurement with the $\mathrm{H} \to \gamma\,\gamma$ decay branching ratio measured at future $\mathrm{e^+e^-}$ Higgs factories.

Acknowledgments – P. R. T. acknowledges financial support from the CERN TH Department and from the FCC project. We thank I. Helenius and L. Harland-Lang for useful discussions on PYTHIA 8 and/or photon-photon collisions, as well as J. Jowett for feedback on running conditions for light-ions at the HL-LHC and HE-LHC, and to E. Chapon on statistical methods.

References

1. C. von Weizsäcker *Z. Physik* **88** (1934) 612; E. J. Williams, Phys. Rev. **45** (1934) 729. E. Fermi *Nuovo Cimento* **2** (1925) 143.
2. C. A. Bertulani and G. Baur, Phys. Rept. **163** (1988) 299.
3. A. J. Baltz *et al.*, Phys. Rept. **458** (2008) 1. [arXiv:0706.3356 [nucl-ex]]
4. Z. Citron *et al.*, arXiv:1812.06772 [hep-ph]; A. Abada *et al.* [FCC Collab.], CERN-ACC-2018-0059.
5. A. Dainese *et al.*, CERN Yellow Report **3** (2017) 635, doi:10.23731/CYRM-2017-003.635 [arXiv:1605.01389 [hep-ph]]; D. d'Enterria *et al.*, QM'17 Proceeds., Nucl. Phys. A **967** (2017) 888 [arXiv:1704.05891 [hep-ex]]; and A. Abada *et al.* [FCC Collab.], CERN-ACC-2018-0058.
6. M. Grabiak *et al.*, J. Phys. G **15** (1989) L25; E. Papageorgiu, Phys. Rev. D **40** (1989) 92; M. Drees *et al.*, Phys. Lett. B**223** (1989) 454; K. J. Abraham *et al.*, Phys. Lett. B **251** (1990) 186.
7. D. d'Enterria and J. P. Lansberg, Phys. Rev. D **81** (2010) 014004 [arXiv:0909.3047 [hep-ph]].
8. M. G. Albrow *et al.* [FP420 R&D Collab.], JINST **4** (2009) T10001.
9. D. d'Enterria, D. Martins, P. Rebello Teles, CERN-Proceeds-2018-001.33; arXiv:1712.10104 [hep-ph].
10. D. d'Enterria, D. E. Martins and P. Rebello Teles, arXiv:1904.11936 [hep-ph].
11. J. Alwall *et al.*, JHEP **09** (2007) 028 [arXiv:0706.2334 [hep-ph]].
12. M. A. Shifman, A. I. Vainshtein, M. B. Voloshin and V. I. Zakharov, Sov. J. Nucl. Phys. **30**, 711 (1979) [Yad. Fiz. **30** (1979) 1368]; B. A. Kniehl and M. Spira, Z. Phys. C **69** (1995) 77; S. Dawson and R. Kauffman, Phys. Rev. D **49** (1994) 2298.
13. V. M. Budnev, I. F. Ginzburg, G. V. Meledin, V. G. Serbo, Phys. Rept. **15** (1975) 181.
14. J.D. Jackson, *Classical Electrodynamics*, 2nd edition, John Wiley & Sons (1975).
15. H. De Vries, C. W. De Jager and C. De Vries, Atom. Data Nucl. Data Tabl. **36** (1987) 495.
16. R. N. Cahn and J. D. Jackson, Phys. Rev. D **42**, 3690 (1990).
17. M. Spira, Nucl. Instrum. Meth. A **389** (1997) 357; A. Djouadi, J. Kalinowski and M. Spira, Comput. Phys. Commun. **108** (1998) 56; A. Djouadi, J. Kalinowski, M. Mühlleitner and M. Spira, arXiv:1003.1643 [hep-ph]; `http://people.web.psi.ch/spira/hdecay/`.
18. T. Sjöstrand *et al.*, Comput. Phys. Commun. **191** (2015) 159.
19. S. Catani, Y. L. Dokshitzer, M. H. Seymour and B. R. Webber, Nucl. Phys. B **406** (1993) 187.
20. M. Cacciari, G. P. Salam and G. Soyez, Eur. Phys. J. C **72** (2012) 1896. [arXiv:1111.6097 [hep-ph]].